Optical Engineering 45(2), 024402 (February 2006)

Strain transferring analysis of fiber Bragg grating sensors

Dongsheng Li
Hongnan Li
Liang Ren
Gangbing Song*
Dalian University of Technology
Department of Civil and Hydraulic Engineering
State Key Laboratory of Coastal
& Offshore Engineering
116023, China
E-mail: dsli@dlut.edu.cn

Abstract. We develop an analytical model for the relationship between the strain measured by a fiber Bragg grating sensor and the actual structural strain. The values of the average strain transfer rates calculated from the analytical model agree well with available experiment data. Based on the analytical model, the critical adherence length of an optical fiber sensor can be calculated and is determined by a strain lag parameter, which contains both the effects of the geometry and the relative stiffness of the structural components. The analysis shows that the critical adherence length of a fiber sensing segment is the minimum length with which the fiber must be tightly bonded to a structure for adequate sensing. The strain transfer rate of an optical fiber sensor embedded in a multilayered structure is developed in a similar way, and the factors that influence the efficiency of optical fiber sensor strain transferring are discussed. It is concluded that the strain sensed by a fiber Bragg grating must be magnified by a factor (strain transfer rate) to be equal to the actual structural strain. This is of interest for the application of fiber Bragg grating sensors. © *2006 Society of Photo-Optical Instrumentation Engineers.* [DOI: 10.1117/1.2173659]

Subject terms: fiber Bragg grating sensors; strain transferring; critical adherence length; strain transfer rate.

Paper 050091RR received Feb. 4, 2005; revised manuscript received Jun. 15, 2005; accepted for publication Jul. 1, 2005; published online Feb. 27, 2006.

1 Introduction

Fiber Bragg grating (FBG) sensors are becoming promising sensing elements for structural health monitoring of civil structures. In comparison with conventional electric or electromagnetic sensors, FBG sensors exhibit many advantages, such as (1) electromagnetic inference immunity and low energy loss, which is preferable in the applications of long-distance health monitoring; (2) multiplexing ability coded in wavelengths to enable quasi-distributive measurement of strains by one fiber; (3) high sensibility over a large measuring range; and (4) compactness and flexibility with minimum influence on the mass and stiffness properties of the host structure.[1] The past decade has witnessed an intense international research effort in FBG sensors for structural health monitoring and successful demonstrations in a variety of civil structures, especially, bridges.[2] In these applications, the values measured by FBG sensors were assumed to be the actual structural strains.[3] In fact, the strain measured by an FBG sensor is different from the actual host structure strain because of the difference between the optical fiber core modulus and the modulus of the fiber coating or the adhesive. The methods to integrate FBG sensors with host structures can generally be divided into three different categories in terms of packing strategies: (1) direct integration, in which FBG sensors are directly embedded in or surfaced bonded to a host structure; (2) sensor-packaging integration, by which FBG sensors are first fixed in a small tube or bonded on the surface of a plate, and then the tube or the plate is anchored in the host structure; (3) clamping integration, in which an FBG sensor is gripped at two ends by a bracket fixed on the host structure. No matter how the FBG sensors are packaged and integrated, the fiber core where the FBGs are written is brittle and must be protected by adhesives or a coating layer in civil engineering applications to avoid fiber breakage and to ascertain its long term stability. However, such a protection results in inconsistency between the fiber strain and the structural strain. Such discrepancies are neglected in most applications of FBG sensors by simply assuming that the fiber strain is consistent with the host structural strain.[1,4,5] This assumption gives acceptable measurement results for optical fiber sensors (OFSs) with long gauge lengths, in which the peak host strain can be fully transferred into the fiber strain, but cannot provide good measurement strains for short-gauge OFSs, for instance, fiber Bragg grating sensors, in which the effect of the bonded fiber length on strain transfer between the fiber and host structure is significant.[6] It is, thus, of primary importance to have a detailed knowledge of the relationship between the host structural strain and the fiber strain to correctly interpret structural strain from the strains sensed in the fiber.

Since the Young's modulus of the fiber is typically much larger than that of the adhesive or the coating, the axial elastic displacements of the fiber and the host material are different. Pak[7] analyzed the strain transfer of a coated optical fiber embedded in a host composite, which is strained by a far-field longitudinal shear stress parallel to the optical

*Dr. Song is an associate professor with the Department of Mechanical Engineering at University of Houston, Houston, Texas 77204-4006.

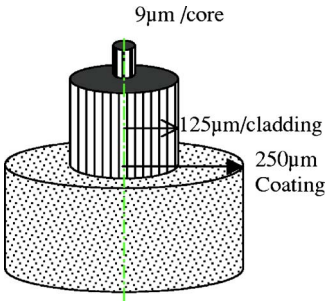

Fig. 1 Structure of a typical single-mode fiber.

fiber. In this case, the maximum shear transfer occurs when the shear modulus of the coating is the geometric mean of the shear moduli of the fiber and the host material. Ansari and Libo[8] obtained axial strain distribution along the fiber length by assuming that the strain at the middle of the bonded fiber is equal to that of the host structure at the same position. Galiotis et al.[6] designed a polydiacetylene single fiber in an epoxy resin host material subjected to tensile strain along the fiber direction, and measured the strains at all points along the length of the fiber by the method of resonance Raman. They found that the axial strain in the fiber rises from a finite value at the end of the fiber to a fairly constant value at the central portion of the fiber, and that the axial strain at the midpoint of the fiber is lower than that applied to the host material, which can be approximately explained by the shear-lag model of Cox.[9] In this model, the composites are assumed to contain many fibers.

This paper mainly concerns the theoretical study of a single optical fiber embedded in a finite host structure, which is subjected to uniform axial stress. To derive the relationship between the strain measured by a fiber Bragg grating sensor and the actual one experienced by the structure, a more realistic hypothesis is proposed in this paper. The theoretical study found that the maximum strain transferred from the host to fiber at its middle length does not necessarily equal that of the host structure. The average strain along the gauge length depends on the length of the fiber in contact with the host structure and the mechanical properties of the fiber and the layer between the fiber and the host structure. The influence of the difference in elastic moduli between the fiber and the adhesive or coating layer on the critical adhesion length is investigated. The strain transfer rates predicted by the developed mode are consistent with the available experimental data. Finally, the developed model is extended to the case where several middle layers exist between the fiber and host material.

2 Theoretical Approach

An optical fiber usually consists of three layers: fiber core, cladding, and coating. The core diameter of a single-mode fiber, often employed in civil engineering, is 9 μm, and the value for a multiple-mode fiber is 50 μm (Fig. 1). The coating, i.e., the outer layer of an optical fiber, often has an outer diameter of 250 μm and an inner diameter of 125 μm. The majority of optical fibers used in sensing applications have silica glass cores and claddings. The coating is usually made of plastics to provide the fiber with sufficient mechanical strength and to protect it from damage or moisture absorption. The refractive index of the cladding is lower than that of the core to satisfy the conditions of Snell's law and to ensure a total internal reflection and confine the propagation of the light within the fiber core. A Bragg grating is a permanent periodic modulation of the refractive index in the core of a single mode optical fiber. The phase mask technique[10] is commonly used to transversely write a Bragg grating. A typical change in the refractive index of the core is between 10^{-5} and 10^{-3}, and the length of a Bragg grating is typically around 10 mm. When light transmitted in a fiber impinges on Bragg gratings, constructive interference between the forward wave and the contrapropagating wave leads to a narrowband back-reflection of light when the Bragg (or phase match) condition is satisfied. The Bragg condition can be expressed by the following relationship between the central wavelength of a Bragg grating and its period[11]

$$\lambda_b = 2n\Lambda, \tag{1}$$

where λ_b, n, and Λ are, respectively, the central wavelength, effective refractive index, and the period of a Bragg grating. (See Table 1 for a summary of the notation used in this paper.)

The strain applied to a Bragg grating alters its period, and thus changes the wavelength of the reflected light. In general, the Bragg wavelength of the reflected light varies with the applied strain as follows:[1,4]

$$\frac{1}{\lambda_b}\frac{\Delta\lambda_b}{\epsilon} = 0.78 \times 10^{-6}/\mu\epsilon. \tag{2}$$

Hence, the fiber strain can be obtained by measuring the change of the reflected light wavelength. Once the relationship between the fiber strain and the host structure strain is established, the structural strain can be directly acquired from the Bragg wavelength change according to Eq. (2) since the Bragg wavelength of the reflected light can be readily measured.

FBG sensors have a unique property as compared with other OFSs in that they encode the wavelength, which is an absolute parameter and does not suffer from disturbances of the light paths. FBG sensors can be used to measure the strains of multiple locations of a structure if many gratings with different periods are arranged along an optical fiber. In this configuration, each of the reflected signals has a unique wavelength and can be easily monitored, thus achieving multiplexing of the outputs of multiple sensors using a single fiber. Currently, up to 64 FBGs can be commercially wavelength-multiplexed in one fiber,[12] which enables quasi-distributive measurement of strains and makes FBG sensors most suitable for structural health monitoring of large civil structures.

A more accurate model describing the relationship between the strain sensed by a Bragg grating and the actual structural strain is developed in this paper. This model is suitable for two different cases. In the first case, a fiber with coating is directly embedded in the host structure. In the second case, the coating of a fiber is first stripped off, and then the bare fiber (including the core and cladding only) is attached to the inner surface of a steel tube by adhesives. In

Table 1 Symbols used in this paper.

Symbol	Meaning
C_1, C_2	Constants of integration
E_c	Young's modulus of the coating or adhesive
E_g	Young's modulus of the fiber
G_c	Shear modulus of the coating or adhesive
k	Strain lag parameter
k_m	Strain lag parameter for a multiple layer model
L	Half of optical fiber gauge length
l_c	Half critical adherence length
r_i	Radius of the ith layer
r_g, r_m	Radius of fiber, inner radius of host material
u	Axial displacement
w	Radial displacement
α	Ratio between fiber strain and host strain
α_m	Maximum ratio between fiber strain and host strain
$\gamma(x, r)$	Shear strain
n	Effective refractive index of optical fiber
μ	Poisson's ratio
ϵ	Strain
λ	Wavelength of light
λ_b	Wavelength of light reflected by Bragg gratings
σ	Axial stress
τ	Shear stress
Subscripts	

Symbol	Meaning
m, c, g	Strain, stress related to host material, coating, glass fiber, respectively
i	Layer index for a multiple model

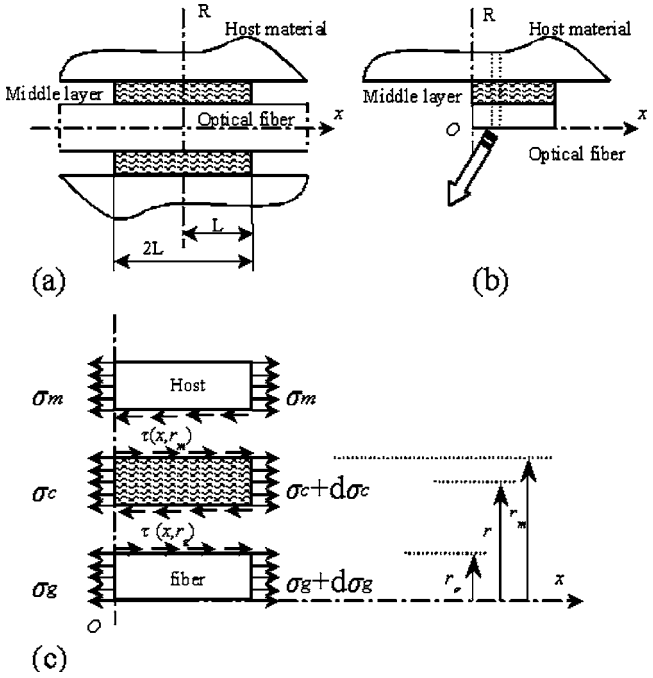

Fig. 2 Coordinate system and free-body diagram of symmetrical section of optical fiber: (a) optical fiber of gauge length 2L, (b) one quarter of the fiber; and (c) stress distribution of the fiber and the coating.

these two cases, there is an adhesive layer, often called middle layer, between the bare fiber and the host material. The three layers are concentric and the strain of the outer host material is transmitted to the inner fiber through the deformations of the middle layer.

In the analysis of strain transfer to the optical fiber from the host material, the following assumptions are adopted in this paper:

1. All the materials pertinent to the model remain elastic, and only the outer host material is subjected to axial stress and is uniformly strained, whereas the bare fiber and the middle layer do not directly bear any external loadings.
2. Mechanical properties of the core and cladding of the fiber are the same. In reality, their properties are slightly different owing to their difference in some chemical components and the writing process of Bragg gratings. The core and cladding, hereinafter, are referred collectively as fiber for simplicity.
3. There are no strain discontinuities across the interfaces, including the one between the host material and the middle layer and the one between middle layer and fiber interfaces, i.e., the bond between all the interfaces is perfect and no debonding exists.

In this paper, we consider a single optical fiber of Young's modulus E_g and radius r_g embedded in a host material, separated by a middle layer of Young's modulus E_c and radius r_m and Poisson's ratio μ, as illustrated in Fig. 2. The host material, assumed to be infinite in all directions, is subjected to a uniform axial stress. Here, L is the half gauge length of an optical fiber sensor, and 2L is the total length

that the fiber is bonded to the host material through the middle layer; $\tau(x,r)$ is the shear stress in the middle layer a distance r above a given x coordinate along the center of the fiber; $\tau(x,r_g)$ is the shear stress at a given x coordinate along the fiber-middle layer interface; σ_g, σ_c, and σ_m are the axial stress in the fiber, the middle layer, and the host material, respectively.

Based on the stress equilibrium for a small segment of the fiber and assumptions 1 to 3, the longitudinal stress along the fiber σ_g, is related to the interfacial shear stress at the fiber/middle layer interface through[13]

$$\frac{d\sigma_g}{dx} = -\frac{2\tau(x,r_g)}{r_g}. \tag{3}$$

In reference to the free-body diagram pertaining to the middle layer [Fig. 2(c)], the equilibrium in the x direction results in the following relationship by balancing the shear stresses $\tau(x,r_g)$ and $\tau(x,r_m)$ with the axial stress σ_c:

$$\tau(x,r) = \frac{r_g}{r}\tau(x,r_g) - \frac{r^2 - r_g^2}{2r}\frac{d\sigma_c}{dx}. \tag{4}$$

Substitution of Eq. (3) into Eq. (4) leads to

$$\tau(x,r) = -\frac{r_g^2}{2r}\frac{d\sigma_g}{dx} - \frac{r^2 - r_g^2}{2r}\frac{d\sigma_c}{dx}. \tag{5}$$

Since the shear modulus of deformation predominates when it comes to the load transferring between the host material and the fiber, lateral motions perpendicular to the x coordinate are of secondary importance for the present study, and the Poisson effect can be neglected without much error. Using the constitutive equation relating stress to strain, $\sigma_g = E_g\epsilon_g$, where $\epsilon_g = du/dx$ is the axial strain along the fiber, and $u = u(x)$ is the displacement, we obtain,

$$\tau(x,r) = -\frac{r_g^2}{2r}E_g\frac{d\epsilon_g}{dx} - \frac{r^2 - r_g^2}{2r}E_c\frac{d\epsilon_c}{dx} = -\frac{E_g r_g^2}{2r}\left(\frac{d\epsilon_g}{dx} - \frac{r^2 - r_g^2}{r_g^2}\frac{E_c}{E_g}\frac{d\epsilon_c}{dx}\right). \tag{6}$$

Since the fiber is strained together with the middle layer, the strain gradients are expected to be of the same order:

$$\frac{d\epsilon_g}{dx} \cong \frac{d\epsilon_c}{dx}. \tag{7}$$

Thus, the important factor that determines $\tau(x,r)$ in Eq. (6) is the ratio of the stiffness between the fiber and the middle layer. The Young's modulus of the optical fiber coatings, in the case of a coated fiber, or the Young's modulus of typical structural epoxies, in the instance of a bare embedded fiber is, as usual, 10% or less than that of the glass fiber, and r is not much larger than r_g (the middle layer is typically very thin to admit efficient strain transfer between the fiber and the host material), the second part of the right-hand side of Eq. (6) is, therefore, insignificant compared to the first part:

$$\frac{r^2 - r_g^2}{r_g^2}\frac{E_c}{E_g}\frac{d\epsilon_c}{dx} \cong o\left(\frac{d\epsilon_g}{dx}\right). \tag{8}$$

Substituting Eqs. (7) and (8) into Eq. (6) results in

$$\tau(x,r) = -\frac{r_g^2}{2r}\frac{d\sigma_g}{dx} = -\frac{r_g^2}{2r}E_g\frac{d\epsilon_g}{dx}. \tag{9}$$

The shear stress term in Eq. (9) is determined by using Hooke's law as follows:[13]

$$\tau(x,r) = G_c\gamma(x,r) = G_c\left(\frac{\partial u}{\partial r} + \frac{\partial w}{\partial x}\right) \cong G_c\frac{\partial u}{\partial r}, \tag{10}$$

where $u = u(x)$ and $w = w(x)$ are the axial and radial displacements in the middle layer, respectively. Substituting Eq. (10) into Eq. (9) and integrating the resulting expression over r_g from the fiber and middle layer interface to the middle layer and host material interface radius r_m gives

$$\int_{r_g}^{r_m}\left(G_c\frac{\partial u}{\partial r}\right)dr = \int_{r_g}^{r_m}\left(-\frac{r_g^2}{2r}E_g\frac{d\epsilon_g}{dx}\right)dr. \tag{11}$$

The integration result of Eq. (11) is

$$u_m - u_g = -\frac{E_g}{2G_c}\frac{d\epsilon_g}{dx}r_g^2\ln\left(\frac{r_m}{r_g}\right) = -\frac{1}{k^2}\frac{d\epsilon_g}{dx}, \tag{12}$$

where u_m and u_g, respectively, denote the axial displacement from the x coordinate origin in the host material and fiber. The strain lag parameter k containing both effects of the geometry and the relative stiffness on the system components, can be written as

$$k^2 = \frac{2G_c}{r_g^2E_g\ln(r_m/r_g)} = \frac{1}{(1+\mu)(E_g/E_c)r_g^2\ln(r_m/r_g)}, \tag{13}$$

where $G_c = E_c/[2(1+\mu)]$, is the shear modulus of the middle layer. Differentiation of Eq. (12) with respect to x yields

$$\frac{d^2\epsilon_g(x)}{dx^2} - k^2\epsilon_g(x) = -k^2\epsilon_m. \tag{14}$$

The general solution to Eq. (14) takes of the following form:

$$\epsilon_g(x) = c_1e^{kx} + c_2e^{-kx} + \epsilon_m, \tag{15}$$

where c_1 and c_2 represent the integration constants determined by boundary conditions. Since the host material does not contact the fiber beyond the ends of the interface between the fiber and the middle layer, the fiber is assumed to be free from axial stress at both ends. This assumption means that the strain transferred to the fiber is equal to zero at both ends of the OFS, and is given by

$$\epsilon_g(L) = \epsilon_g(-L) = 0. \tag{16}$$

The boundary conditions established by Eq. (16) are identical to the following equations:

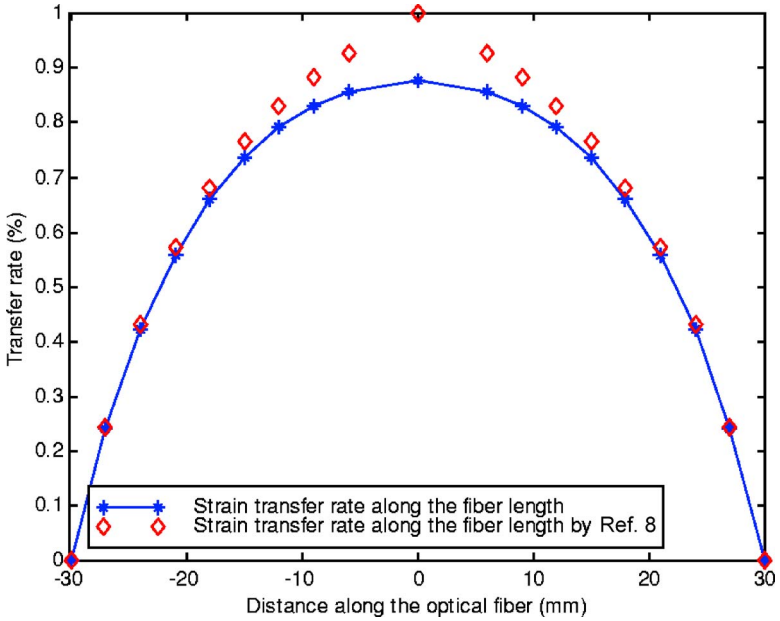

Fig. 3 Distribution of normal strain in fiber along the length.

$$\epsilon_g(L)=0, \quad \sigma_g(0)=0, \quad \text{or } \epsilon_g(0)=0. \tag{17}$$

The relationship of Eq. (17) states that there is no shear stress in the fiber at the midpoint of the fiber [refer to Eq. (3)] due to the symmetric nature of the structure. The boundary conditions established in Eqs. (16) and (17) will lead to the same solution as Eq. (15). Hence, by imposing these boundary conditions on Eq. (15), c_1 and c_2, are evaluated and obtained as

$$c_1=c_2=-\frac{\epsilon_m}{2\cosh(kL)}. \tag{18}$$

Thus, the final solution to Eq. (15), i.e., the strain distribution along fiber and its relationship to the strain of the host material at a given x coordinate, is

$$\epsilon_g(x)=\epsilon_m\left[1-\frac{\cosh(kx)}{\cosh(kL)}\right]. \tag{19}$$

Equation (19) is the governing equation that describes the strain distribution along the fiber. The effects of the Young's moduli of the fiber and the middle layer, as well as the effects of the radii of the fiber and the middle layer, on the strain transfer, are all included in the strain lag parameter k defined in Eq. (13).

Figure 3 shows the strain transfer rate along an optical fiber. The mechanical properties of the optical fiber employed in this paper, are given in Table 2. These properties are the same as those used by Ansari and Libo[8] for comparison purposes. The strain difference between the fiber and the host material at a given x coordinate, is determined by the strain lag parameter k. Figure 3 also demonstrates that the strain sensed by the fiber at the midpoint is not equal to the strain in the host material in this instance. Our results agree with the conclusions drawn by other authors in different forms.[14,15] However, in the work by Ansari and Libo[8], these two strain values are assumed equal.

In general, the bonded section of an FBG is typically shorter than 60 mm, and thus the strain of the fiber at the midpoint deviate considerably from the host material strain. If the assumption by Ansari and Libo[8] is used in such cases, there will be more errors. This phenomena can be seen in the experiments by Galiotis et al.[6] in which the maximum strain transferred to fiber I lagged about 0.6% and 0.7 to 0.8% in fiber Π from the host material strain. These observations are in sharp contrast to the assumption made in the analytical approach[8] that the fiber strain at the midpoint is equal to the host material strain, $\sigma_g/E_g=\sigma_m/E_m$. The experimental results by Galiotis et al.[6] also indicate that the lagging of the fiber strain from the host materials varies with the bonded fiber lengths.

3 Average Strain Transfer Rate

The strain transferred from the host material to an optical fiber varies with the different points along the gauge length of the fiber. Strain transfer rate (STR) $\alpha(x)$ can be defined

Table 2 Mechanical properties of the optical fiber.

Materials Properties (1)	Symbols (2)	Values (3)	Unit (4)
Young's modulus of the fiber	E_g	7.2×10^{10}	Pa
Young's modulus of silicon coating	E_c	2.55×10^{6}	Pa
Poisson's ratio of silicon coating	μ	0.48	—
Shear modulus of silicon coating	G_p	8.5×10^{5}	Pa
Radius of outer boundary of silicon coating	r_m	102.5	μm
Radius of the fiber	r_g	62.5	μm

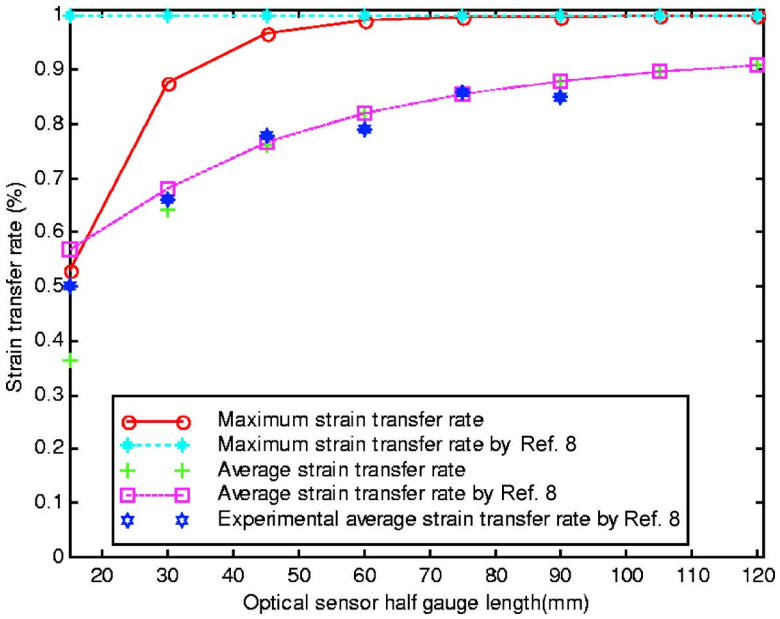

Fig. 4 Comparison of maximum STR and ASTR with experimental data for various gauge length sensors.

as the ratio of the strain measured by an FBG sensor and the strain actually experienced by the host material at a given point of the fiber (a given x coordinate) as follows:

$$\alpha(x) = \frac{\epsilon_g(x)}{\epsilon_m} = 1 - \frac{\cosh(kx)}{\cosh(kL)}. \tag{20}$$

The maximum STR $\alpha_m(x)$ happens at the midpoint of the fiber, i.e., at the point where x is equal to zero:

$$\alpha_m(0) = \frac{\epsilon_g(0)}{\epsilon_m} = 1 - \frac{1}{\cosh(kL)}. \tag{21}$$

Generally, the strain measured by an FBG sensor, is the average strain over the gauge length of the fiber. Average STR (ASTR) can be expressed in the following form:

$$\bar{\alpha} = \frac{\overline{\epsilon_g(x)}}{\epsilon_m} = \frac{2\int_0^L \epsilon_g(x)\,\mathrm{d}x}{2L\epsilon_m} = 1 - \frac{\sinh(kL)}{kL\cosh(kL)}. \tag{22}$$

The ASTR determined by Eq. (22) depends only on the gauge length and the mechanical properties of the optical fiber and the middle layer. Therefore, it can be readily employed for correct interpretation of structural strains from the optical fiber measurement values under the Assumptions 1 to 3 in Sec. 2. The results from the developed analytical model can be used as a complement to experiments especially where calibration tests are difficult to perform or where qualitative interpretation of a measurement system is required, for instance, in embedment applications of FBG sensors. Note also that the preceding analysis is also applicable to evaluate the displacement OFSs based on Michelson interference principle in Ref. 8.

Figure 4 shows the variation of ASTRs α over the fiber length and maximum STRs at the midpoint of the fiber in terms of the gauge length of the optical fiber, and also the experimental values by Ansari and Libo.[8] It can be seen that the ASTRs and maximum STRs for the optical fiber in our study differs from those derived by Ansari and Libo,[8] especially for the optical fiber with half-gauge length shorter than 60 mm. When the fiber gauge length increases, the ASTRs and the maximum STRs determined by Ansari and Libo[8] are close to the values presented in this paper since sinh (kL) is nearly equal to cosh(kL) for a larger fiber half gauge length L. Note that Eq. (22) is a more accurate solution for the strain transfer problem in the concentric cylinder model.

As indicated in Fig. 4, the ASTR experimental values by Ansari and Libo[8] agree quite well with those evaluated by Eq. (22). Although the model has been verified for the simple case in this paper, further experiments are required to validate its generalization. In any case, it facilitates a simple and direct qualitative interpretation of structural strains from measurement values made by OFSs.

Since the STRs at all the points within the fiber gauge length varies and a Bragg grating demands uniform axial deformations to avoid multiple-peak reflection and light spectrum expansion, it is required that an optical fiber be evenly stressed. However, only a short portion of FBG sensor is usually bonded, and this will lead to inadequate strain transfer, i.e., the strain sensed by a FBG sensor is only a fraction of the host material strain. Figure 5 shows the variation of ASTRs α along the fiber with a gauge length 120 mm. The figure indicates that the STRs near the center of the fiber approach unity. Therefore, an adequate fiber length must be bonded to ensure the correct measurement of the host structural strain. Critical adherence length (CAL) can be defined as the minimum length to be bonded so that the STRs, at least over the middle half-length of the fiber, are larger than 0.9, i.e.,

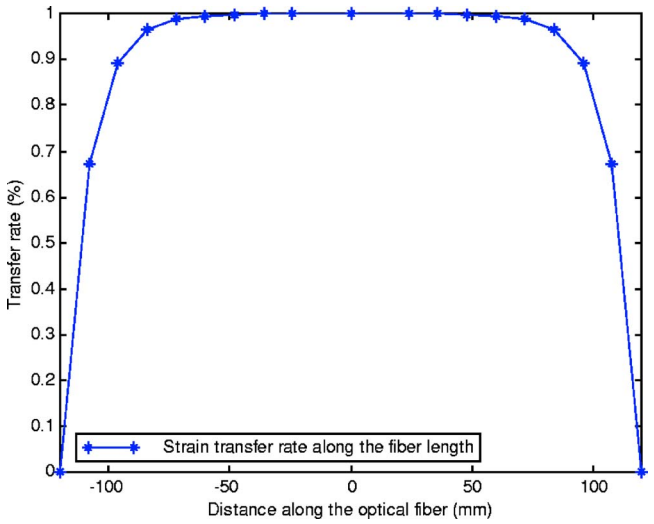

Fig. 5 Strain transfer rate of a 120-mm-gauge-length fiber.

$$\alpha(l_c/2) \geqslant 0.9. \tag{23}$$

Substituting Eq. (20) into Eq. (23) gives

$$\frac{\epsilon_g(l_c/2)}{\epsilon_m} = 1 - \frac{\cosh(kl_c/2)}{\cosh(kl_c)} \geqslant 0.9. \tag{24}$$

The solution of Eq. (24) is

$$\mathrm{CAL} = l_c = 9.24/k, \tag{25}$$

where l_c is only computed over the half gauge length. Critical adherence length means that an OFS can be bonded over a longer portion, and the effective gauge length is located in the middle. For the case shown in Table 2, the CAL is 99.78 mm. This implies that the STRs along the middle half-length of the fiber are larger than 0.9 as long as the minimum bonded fiber length is beyond 99.78 mm. CAL indicates that we can bond an FBG over a longer length, for instance 80 mm, to locate the FBG just in the middle of the adhered length for efficient strain transferring.

4 Strain Transferring for a Multilayered Concentric Model

In many cases, there are several middle layers between the fiber and host material, for instance, the fiber is first coated with an adhesive that solidifies quickly, and then bonded to the structure by an epoxy that solidifies slowly to ensure a uniform stress distribution. One typical case is to bond the fiber to a structure by directly applying adhesives on the fiber coating, and the coating and the adhesive form two separate layers between the fiber and host material. In some sensing applications, specialized coatings are required to enhance an optical fiber's measurement sensitivity and to accommodate the host structure. The FBGs used in this paper are coated in this way with two different layers of coatings to employ their advantages of mechanical properties.

Figure 6 shows a multiple layer model available for the strain transfer analysis. Additionally, r_i is the outer radius

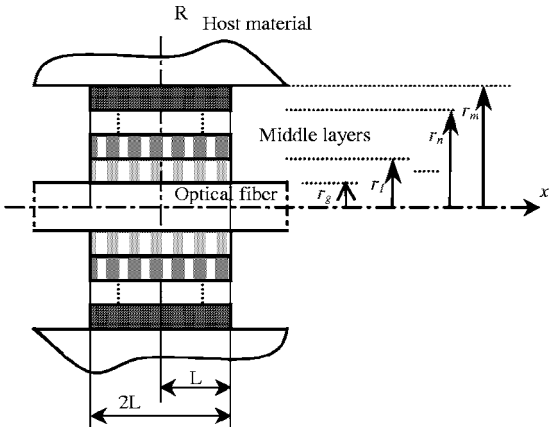

Fig. 6 Cross section of a multilayer adhered fiber.

of the ith layer ($i=1$ to n), r_g is the outer radius of the fiber layer, and r_m is the inner radius of the host materials [i.e., the outer radius of the $(n+1)$th layer]. Here G_i is the shear modulus of the ith layer ($i=2$ to n), and G_c is the shear modulus of the first layer.

Equation (11) can be rewritten as

$$\int_{r_g}^{r_m}\left(\frac{\mathrm{d}x}{\mathrm{d}r}\right)\mathrm{d}r = \int_{r_g}^{r_m}\left(-\frac{1}{G_c}\frac{r_g^2}{2r}E_g\frac{\mathrm{d}\epsilon_g}{\mathrm{d}x}\right)\mathrm{d}r. \tag{26}$$

The resulting expression is integrated, over r_g, from the fiber and first layer interface, to the outmost layer and host material interface radius r_m through all the middle layers as follows:

$$\left[\int_{r_g}^{r_1} + \int_{r_1}^{r_2} + \cdots + \int_{r_n}^{r_m}\left(\frac{\mathrm{d}x}{\mathrm{d}r}\right)\right]\mathrm{d}r = \left[\int_{r_g}^{r_1} + \int_{r_1}^{r_2} + \cdots + \int_{r_n}^{r_m}\left(-\frac{1}{G_c}\frac{r_g^2}{2r}E_g\frac{\mathrm{d}\epsilon_g}{\mathrm{d}x}\right)\mathrm{d}r\right]. \tag{27}$$

The integration result of Eq. (11) is given by

$$u_m - u_g = -\frac{1}{k_m^2}\frac{\mathrm{d}\epsilon_g}{\mathrm{d}x} = -r_g^2\frac{E_g}{2}\left[\sum_{i=2}^{n}\frac{1}{G_i}\ln\left(\frac{r_i}{r_{i-1}}\right) + \frac{1}{G_c}\ln\left(\frac{r_1}{r_g}\right)\right]\frac{\mathrm{d}\epsilon_g}{\mathrm{d}x}, \tag{28}$$

where u_m and u_g denotes the axial displacement from the x coordinate origin in the host material and fiber, respectively:

$$k_m^2 = \frac{2}{r_g^2E_g\left[\sum_{i=2}^{n}(1/G_i)\ln(r_i/r_{i-1}) + (1/G_c)\ln(r_1/r_g)\right]}. \tag{29}$$

The strain lag parameter k, similar to the formerly discussed case, is determined by Young's moduli of the fiber and the middle layers, and the diameters of the fiber and the middle layers.

Thus, Eqs. (20) and (29) can be used directly to compute the strain transfer rate for a fiber embedded in host material with multiple layers. Consequently, the critical adherence length and the average strain transfer rate within a gauge length for an optical fiber sensor can be computed by Eqs. (20) and (29).

5 Conclusions and Discussion

The average strain transfer rate was analytically derived for an optical fiber embedded in a host structure separated by a middle layer. The values of the average strain transfer rates calculated from the analytical model agree well with available experiment data. This enables simple and direct qualitative interpretation of structural strains from measurements made by OFSs, especially when calibration tests are difficult or impossible to perform.

Moreover, the critical adherence length of an optical fiber sensor, which shows the influence of the middle layer on the strain transfer rate, was defined. Consequently, some measures were suggested to make the strain transfer more efficient for the packaging and installing of optical fiber sensors.

More experiments with different middle layers should be performed in the future to further the generalization of the model developed in this paper. And this model may also be extended to the case of arbitrary strain loads, or even in the case of loads in arbitrary directions.

Acknowledgments

The authors are grateful for the works of Prof. Farhad Ansari and their experiments, by which the presented work was motivated. The authors are also grateful for the joint support of China Natural Science Foundation (No. 50408031), the Natural Science Foundation of LiaoNing (No. 20032120, 20042149), the Construction Administration of LiaoNing (No. 02001), and Young Teacher's Foundation, Dalian University of Technology.

References

1. E. Udd, *Optical Fiber Smart Structures*, Wiley, New York (1995).
2. R. C. Tennyson, A. A. Mufti, S. Rizkalla, G. Tadros, and B. B. Benmokrane, "Structural health monitoring of innovative bridges in Canada with fiber optic sensors," *Smart Mater. Struct.* **10**, 560–573 (2001).
3. C. Baldwin, T. Poloso, P. Chen, J. Niemczuk, J. Kiddy, and C. Ealy, "Structural monitoring of composite marine piles using optical fiber sensors," in *Smart Structures and Materials and Nondestructive Evaluation for Health Monitoring and Diagnostics*, *Proc. SPIE* **4330**, 487–497 (2001).
4. E. J. Friebele, C. G. Askins, A. B. Bosse, A. D. Kersey, H. J. Patrick, W. R. Pogue, M. A. Putnam, W. R. Simon, F. A. Tasker, W. S. Vincent, and S. T. Vohra, "Optical fiber sensors for spacecraft applications," *Smart Mater. Struct.* **8**, 813–838 (1999).
5. R. M. Measures, *Structural Monitoring with Fiber Optic Technology*, Academic Press, San Diego, CA (2001).
6. C. Galiotis, R. J. Young, P. H. J. Yeund, D. N. Batchelder, "The study of model polydiacetylene/epoxy composites. Part 1: The axial strain in the fibre," *J. Mater. Sci.* **19**, 3640–3648 (1984).
7. E. Y. Pak, "Longitudinal shear transfer in optical fiber sensors," *Smart Mater. Struct.* **1**, 57–62 (1992).
8. F. Ansari and Y. Libo, "Mechanics of bond and interface shear transfer in optical fiber sensors," *J. Eng. Mech.* **124**(4), 385–394 (1998).
9. H. L. Cox, "The elasticity and strength of paper and other fibrous materials," *Br. J. Appl. Phys.* **3**, 72–79 (1952).
10. K. O. Hill and M. Gerald, "Fiber Bragg grating technology: fundamentals and overview," *J. Lightwave Technol.* **15**(8), 1263–1276 (1997).
11. A. D. Kersey, M. A. Davis, H. J. Patrick, M. LeBlanc, K. P. Koo, C. G. Askins, M. A. Putnam, and E. J. Friebele, "Fiber grating sensors," *J. Lightwave Technol.* **15**(8), 1442–1463 (1997).
12. H.-N. Li, D.-S. Li, and G.-B. Song, "Recent applications of fiber optic sensors to health monitoring in civil engineering," *Eng. Struct.* **26**(11), 1647–1657 (2004).
13. S. P. Timoshenko, *Mechanics of Materials*, Vannstrand Reinhold Company, New York (1972).
14. G. Duck and M. LeBlanc, "Arbitrary strain transfer from a host to an embedded fiber-optic sensor," *Smart Mater. Struct.* **9**, 492–497 (2000).
15. C. K. Y. Leung, X. Wang, and N. Olson, "Debonding and calibration shift of optical fiber sensors in concrete," *J. Eng. Mech.* **126**(6), 300–307 (2000).

Dongsheng Li is a lecturer with the Center for Structural Health Monitoring and Control, Dalian University of Technology. His current research interests are fiber Bragg grating sensoring, random loading identification, structural health monitoring, and damage identification, including optimal sensor placement, and damage identification algorithms. He authored and coauthored more than 10 papers.

Hongnan Li is a professor and dean of the School of Civil and Hydraulic Engineering, Dalian University of Technology. He directs the Center for Structural Health Monitoring and Control and is a professor with the Cheung Kong Scholar Program. Li is also a steering member of Evaluation Committee, a member of China Society of Civil Engineering, and a steering member of the Stochastic Vibration Branch of China Society of Vibration Engineering, the Seismic Disaster Prevention Branch of China Society of Buildings, and the Structural Control Branch of China Society of Vibration Engineering. He carried out more than 20 research projects, has published 4 books and more than 140 papers, and has received more than 10 science and technology awards.

Liang Ren received his BS and MS degrees from Department of Physics, Dalian University of Technology, in 2000 and 2003, respectively. His research interests are optic fiber sensor and structural health monitoring.

Gangbing Song a SPIE member, is an associate professor of mechanical engineering with the University of Houston and a National Science Foundation (NSF) CAREER award recipient for 2001. Dr. Song is also a guest professor at Dalian University of Technology, China. He received his PhD and MS degrees from the Department of Mechanical Engineering, Columbia University, New York, in 1995 and 1991, respectively. Dr. Song received his BS degree in 1989 from Zhejing University, China. His research interests are smart materials and structures, structural vibration control, advance control methods, and structural health monitoring. He has developed two new courses in smart materials and published more than 40 journal and more than 80 conference papers. Dr. Song is also a coinventor of a U.S. patent.